(12) INTERNATIONAL APPLICATION PUBLISHED UNDER THE PATENT COOPERATION TREATY (PCT)

(19) World Intellectual Property Organization
International Bureau

(43) International Publication Date
19 November 2009 (19.11.2009)

PCT

(10) International Publication Number
WO 2009/140628 A1

(51) International Patent Classification:
C09D 1/00 (2006.01)

(21) International Application Number:
PCT/US2009/044195

(22) International Filing Date:
15 May 2009 (15.05.2009)

(25) Filing Language: English

(26) Publication Language: English

(30) Priority Data:

61/053,574	15 May 2008 (15.05.2008)	US
61/169,618	15 April 2009 (15.04.2009)	US
12/466,323	14 May 2009 (14.05.2009)	US

(71) Applicant *(for all designated States except US)*: **APPLIED NANOTECH HOLDINGS, INC.** [US/US]; 3006 Longhorn Blvd., Suite 107, Austin, Texas 78758 (US).

(72) Inventors; and

(75) Inventors/Applicants *(for US only)*: **LI, Yunjun** [CN/US]; 11607 Queens Way, Austin, Texas 78759 (US). **ROUNDHILL, David Max** [US/US]; 13325 Black Canyon Drive, Austin, Texas 78729 (US). **YANG, Mohshi** [US/US]; 10201 Spicewood Mesa, Austin, TX 78759 (US). **PAVLOVSKY, Igor** [RU/US]; 1027 Horne Drive, Cedar Park, TX 78613 (US). **FINK, Richard Lee** [US/US]; 9306 Rolling Oaks Trail, Austin, TX 78750 (US). **YANIV, Zvi** [US/US]; 4506 Aqua Verde Drive, Austin, TX 78746 (US).

(74) Agents: **KORDZIK, Kelly, K.** et al.; Fish & Richardson P.C., P.O. Box 1022, Minneapolis, MN 55440-1022 (US).

(81) Designated States *(unless otherwise indicated, for every kind of national protection available)*: AE, AG, AL, AM, AO, AT, AU, AZ, BA, BB, BG, BH, BR, BW, BY, BZ, CA, CH, CN, CO, CR, CU, CZ, DE, DK, DM, DO, DZ, EC, EE, EG, ES, FI, GB, GD, GE, GH, GM, GT, HN, HR, HU, ID, IL, IN, IS, JP, KE, KG, KM, KN, KP, KR, KZ, LA, LC, LK, LR, LS, LT, LU, LY, MA, MD, ME, MG, MK, MN, MW, MX, MY, MZ, NA, NG, NI, NO, NZ, OM, PG, PH, PL, PT, RO, RS, RU, SC, SD, SE, SG, SK, SL, SM, ST, SV, SY, TJ, TM, TN, TR, TT, TZ, UA, UG, US, UZ, VC, VN, ZA, ZM, ZW.

(84) Designated States *(unless otherwise indicated, for every kind of regional protection available)*: ARIPO (BW, GH, GM, KE, LS, MW, MZ, NA, SD, SL, SZ, TZ, UG, ZM, ZW), Eurasian (AM, AZ, BY, KG, KZ, MD, RU, TJ, TM), European (AT, BE, BG, CH, CY, CZ, DE, DK, EE, ES, FI, FR, GB, GR, HR, HU, IE, IS, IT, LT, LU, LV, MC, MK, MT, NL, NO, PL, PT, RO, SE, SI, SK, TR),

[Continued on next page]

(54) Title: PHOTO-CURING PROCESS FOR METALLIC INKS

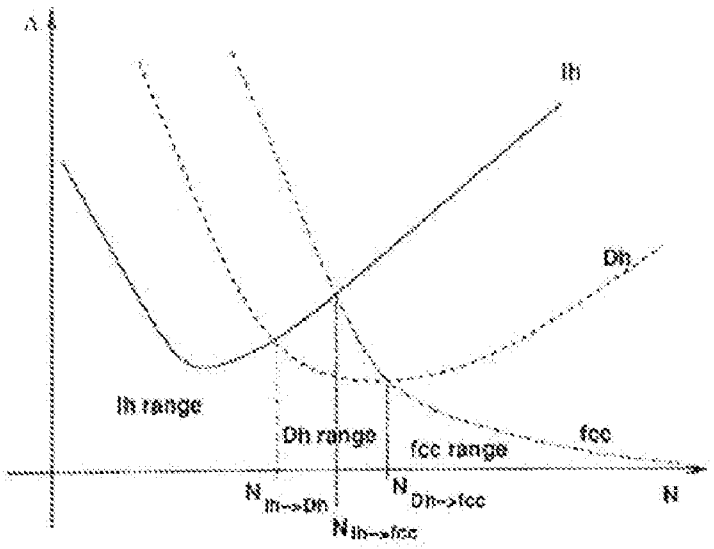

FIG. 1

(57) Abstract: A solution of metal ink is mixed and then printed or dispensed onto the substrate using the dispenser. The film then is dried to eliminate water or solvents. In some cases, a thermal curing step can be introduced subsequent to dispensing the film and prior to the photo-curing step. The substrate and deposited film can be cured using an oven or by placing the substrate on the surface of a heater, such as a hot plate. Following the drying and/or thermal curing step, a laser beam or focused light from the light source is directed onto the surface of the film in a process known as direct writing. The light serves to photo-cure the film such that it has low resistivity.

WO 2009/140628 A1

OAPI (BF, BJ, CF, CG, CI, CM, GA, GN, GQ, GW, ML, MR, NE, SN, TD, TG).

Published:

— *with international search report (Art. 21(3))*

PHOTO-CURING PROCESS FOR METALLIC INKS

This application claims priority to U.S. Provisional Patent Application Serial Nos. 61/053,574 and 61/169,618, which are hereby incorporated by reference herein.

Technical Field

The present invention relates in general to metallic inks for producing conductive paths for electronic circuitry.

Background

The purpose of nanotechnology and science is to understand, control and manipulate objects of a few nanometers in size. These nano-objects are known to behave as an intermediate between single atoms and molecules and bulk matter. These properties are often peculiar and different from the properties of bulk material; in particular, these nano-objects can present properties that vary dramatically with size. This opens the possibility of controlling these properties by precisely controlling their formulation process.

Nanoclusters are aggregates of atoms or molecules with an average diameter less than 100 nm and a number of constituent components ranging from 10 to 10^6. Nanoclusters do not have a fixed size, structure, or composition. As a result, they present a variety of morphologies. Nanoclusters may be homogeneous, which means composed of only one type of atom or molecule, or heterogeneous. The components within a nanocluster may be held together by very different kinds of forces, such as electro-static, Van der Waals, or covalent bonds, depending on the constituent. Small clusters of metal atoms, such as Cu (copper), are held together by forces more like those of covalent bonds, not like the forces exerted by the nearly free electrons of bulk metals. Clusters containing no more than a few hundred metal atoms, resulting in diameters around 3 - 5 nanometers, have strong, size-dependent properties due to quantum confinement. As the cluster becomes larger, with diameters up to 100 nanometers, they possess smooth variations of behavior approaching the bulk size limit.

Nanoclusters usually do not have a crystal lattice structure like their bulk counterparts. These finite clusters can present multiple nanocrystalline structures such as multiple hedronic structures with multiple faces. Some nanoclusters may be a crystalline solid. It is important to understand whether crystalline or noncrystalline structures prevail for a given size and composition in order to describe some physical process involving the nanocluster.

An interesting inquiry for consideration is what happens in a phase transition situation, like copper from liquid to solid, when there are nanoclusters. An answer to this question provides that thermodynamic and kinetic energy stabilities influence. Nanoclusters have a very high surface area to volume ratio resulting in a high surface energy. The nanocluster's structure, including facets, edges and vertices, has a strong influence to this surface energy and thus dominates the nanoparticle's behavior.

In order to fully understand the physical behavior of these nanoclusters several steps are taken. First, nanoparticle structure is the starting point for understanding copper nanocluster behavior. In order to gain a very complicated understanding of the structure-property relationship, a deep study of the minimum energetic situations was performed and the results analyzed. These results are very complicated and convoluted and, until now, has not been done by anyone in the world for copper nanoclusters. Second, is to determine the effect of increased temperature. To answer this question, one must be an expert in the thermodynamics of finite systems. There are very few experts in the world. Third, one needs to understand, in particular for phase transition of copper nanoclusters, what is the time scale in the experimental setting *vs.* the time scale of morphology transitions. Basically, this is solved by the study of kinetic effects in the formation and destruction of nanoclusters.

Brief Description of the Drawings

Figure 1 illustrates qualitative behavior for the excess energy for crystalline, icosahedron and decahedron clusters;

Figure 2 illustrates a particle with a solid core and a surrounding liquid shell;

Figure 3 is a comparison of theoretical and experimental melting points for tin clusters;

Figure 4 illustrates growth simulation for copper nanoclusters;

Figure 5 illustrates graphs of absorption spectra calculated in the dipole approximation for prolate spheroidal Rh and Pt particles in water. The minor diameter of the particles is 10 nm, and the aspect ratios are 1.0 (---), 2.0 (---), 3.0 (---)

Figure 6 illustrates polarization of a spherical metal particle by an electrical field vector of the incoming light;

Figure 7 illustrates absorption spectra of agglomerated (a) and isolated (b) particles of cadmium and thallium in water;

Figure 8 illustrates correlations between average particle size, powder color, ink color, and resistivity after photocuring;

Figure 9 illustrates absorption spectrum of an aged Cd solution before (0) and at various times after exposure to nitrous oxide;

Figure 10 illustrates evidence of reduction of copper oxide to metallic copper in a photo-curing process;

Figure 11A illustrates Sangyo copper nanoparticles (~50 nm) after pre-curing at 100°C in air; Cu/Cu_2O is 2.6:1 (28% Cu_2O);

Figure 11B illustrates Sangyo nanoparticles after photo curing process (the intensity of the Cu_2O peak is significantly reduced; Cu/Cu_2O is 13:1 (7% Cu_2O);

Figure 12A illustrates American Elements copper nanoparticles pre-cured at 100° C in air;

Figure 12B illustrates American Elements copper nanoparticles are photonic-cured at a voltage of 1300 V and bluish color is observed after photonic curing;

Figure 12C illustrates American Elements copper nanoparticles are photonic-cured at a voltage of 1400 V and reddish color is observed after photonic curing;

Figure 13 illustrates a spectrum from a flash xenon lamp;

Figure 14 illustrates drying parameters in accordance with embodiments of the present invention;

Figure 15 illustrates that the electrical properties for samples 3 - 8 are very similar to that of sample 2;

Figure 16 illustrates the percentage blowoff of the copper from the Kapton during a photosintering step;

Figure 17 illustrates drying parameters for each sample;

Figure 18 illustrates that the electrical properties for samples 5 and 7 – 10 are better than that of sample 2;

Figure 19 illustrates the percentage blowoff of the copper from the Kapton during a photosintering step;

Figure 20 illustrates the drying parameters for each sample;

Figure 21 illustrates that samples 2 - 5 had increased resistivity when compared to that of sample 1;

Figure 22 illustrates that samples 3 and 4 had low resistivity while having only 20% blowoff during photosintering;

Figure 23 illustrates electrical properties for the samples;

Figure 24 illustrates drying times;

Figure 25 illustrates percentage blowoff of copper from Kapton during a photosintering process; and

Figures 26A and 26B illustrate a system and method for inkjetting and photo-curing of nanoparticle metal films.

Detailed Description

Surface structure of copper nanoclusters:

In general, the binding energy (E_b) of a cluster of size N with a given structure can be written in the following form:

$$E_b = aN + bN^{2/3} + cN^{1/3} + d \quad (1)$$

where the first term corresponds to the volume contributions and the other represent surface contributions from facets, edges, and vertices (see, T.L. Hill, "Thermodynamics of Small Systems," Parts I and II, 1964, Benjamin, Amsterdam). Volume and surface contributions are in competition. Clusters with low surface energy will have generally a quasi-spherical shape and close packed facets in order to optimize the surface to volume ratio.

From equation (1), one can define a useful parameter that reflects the stability of the cluster with the size N:

$$\Delta(N) = \frac{E_b(N) - N\varepsilon_{coh}}{N^{2/3}} \quad (2)$$

whereby ε_{coh} is the cohesive energy per particle in the bulk solid, and Δ is the excess energy with respect to N atoms in a perfect bulk crystal. For clusters of crystalline structure, the parameter a in equation (1) is simply ε_{coh} so that:

$$\lim_{N \to \infty} \Delta = E_b \quad (3)$$

As illustrated in the graph in Figure 1, in the case of nanocrystalline structures, $a > \varepsilon_{coh}$, and Δ diverges as large sizes.

It is important to understand, empirically and theoretically, what are the different cluster shapes that a solid copper nanocluster can take in order to exactly emulate and calculate the phase transitions from solid to liquid and from liquid to solid in the fusion process that takes place utilizing photonic curing.

The literature provides solutions for building up different shapes with the lowest energy possible (see, A.L. Mackay, 1962, Acta Crystallogr. 15, 916; Martin, T.P., 1996, Phys.Rep.273, 199), such as icosahedra (twenty facets) and decahedra (ten facets).

With respect to copper clusters specifically, some work was done (see, Alonso, J.A., 2000, Chem.Rev. (Washington, D.C.) 100, 637) to understand the energetic properties of small copper nanoclusters. For example, it was found that for $N \leq 10$, there is evidence of possibilities for planar structures (flakes) for small N; as the N grows to around 10^{15}, the icosahedra is favored over the cubical hedron. To understand the energetics of these clusters, very complicated calculations and studies based on density functional calculations (see, Jug, K., B. Zummerman, and A.M.Kostler, 2002, Int.J. Quantum Chem.90. 594) or semi-empirical potential calculations (see, Darby, S., T.V. Mortimer-Jones, R.L. Johnson, and C. Roberts, 2002, J. Chem. Phys. 116, 1536; Doye, J.P., and D.J. Wales, 1998b, New J. Chem. 22, 733) must be performed. In any case, all these calculations compared with some few experimental results show for nanoclusters of copper a prevalence for icosahedra, intermediate sized decahedra, and large face cubic center (fcc) clusters.

Size dependency of the copper nanoparticles melting point:

An important point is to understand the size dependence of the melting point. The size dependency of a nanocluster melting point for a given material usually shows a monotonic decrease with decrease in size and may also show irregular variations.

Consider a cluster of size N and, for simplicity, of spherical shape, at a given pressure p. It is expected then that the melting temperature will be a function of the size $T_m(N)$. Comparison of $T_m(N)$ with $T_m(\infty)$ is then performed, which is the melting temperature of the bulk material. In the case of photo-curing of copper nanoclusters, it is important to study the solid-liquid transitions of these nanoclusters. In order to find a solution to $T_m(N)$, one needs to equate the chemical potential of the solid and of the liquid and solve the equation:

$$\mu_s(p,T) = \mu_l(p,T) \tag{4}$$

This equation means that the chemical potentials of a fully solid and of a fully liquid cluster are equal at melting. After a number of mathematical manipulations (see, Pawlow, P., 1909, Z. Phys. Chem., Stoechiom. Verwandtschaftsl. 65, 1), one obtains the following equation:

$$T_m(N) = T_m(\infty)\{1 - \frac{C}{N^{1/3}}\} \tag{5}$$

where C is a constant and depends on the latent heat of melting per particle, the density of the particle, and interface tensions such as at the solid vapor interface and liquid vapor interface.

This model can be refined by including the possibility of surface melting that may be the case in a photonic curing process. *Id.* In this case, the melting process is considered to start at the surface of a nanocluster as illustrated in Figure 2.

The melting temperature is found by imposing the equilibrium condition on the solid core/liquid shell particle. This model is even further complicated and expanded (see, Kofman, R., P. Cheyssac, A.Aouaj, Y. Lereah, G. Deutscher, T. Ben-David, J.M. Pennison, and A. Bourret, 1994, Surf. Sci. 303, 231) for metallic particles, specifically. In this case, a new variable ξ is introduced that is characteristic to the length of the interaction among atoms and liquid metals in addition to taking into

account the effective interaction between the solid liquid and liquid vapor interfaces. This effective interaction is repulsive and favors the formation of a liquid shell between the solid core and the vapor as illustrated in Figure 2. The equation is much more complex, but it is interesting to see that the simple solution expressed in equation (5) is recovered in the limit $\xi \rightarrow 0$.

It is believed that the solid core/liquid shell model is more accurate and fits the experiment much better. In fact, some researchers (Wang, L., Y. Zhang, X. Bian, and Y. Chen, 2003, Phys.Lett. A 310, 197) discovered that this solid core/liquid shell model fits very well for N = 500 for copper. For example, Figure 3 shows a graph illustrating comparison of theoretical and experimental melting points of tin clusters (see, Lai, S.L., J.Y.Guo, V. Petrova, G. Ramanath, and L.H. Allen, 1996, Phys.Rev. Lett. 77, 99) showing clearly that this approach can theoretically predict the drop in the melting temperature of tin clusters versus size.

Nanoclusters and the melting process in photo-curing:

For the photonic curing process, consider both the melting process of the copper nanoclusters and the formation of the copper nanoclusters in a process of freezing the liquid copper nano-droplets. In particular, the kinetic effects may strongly influence the formation of nanoclusters. An important consideration is the time scale of the copper nanocluster formation. The time scale of nanocluster formation may range from a fraction of a millisecond to a few milliseconds. On this time scale, from the kinetics point of view, clusters may not be able to reach the minimum free energy structure, thus remaining trapped in some meta-stable configuration that has a very long lifetime, especially when the clusters are further cooled down after their solidification, as is the case of the photo-curing process disclosed herein.

In order to build a model and study the formation process of solid clusters of copper in the herein described photo-curing process, solid clusters in contact with a thermal bath are studied. In an embodiment of the present invention, this bath is more complicated, because it includes the substrate and the environment around the substrate.

There are two models for studying the formation of nanoclusters. One is referred to as a liquid state growth model, and is simulated by freezing a liquid droplet

until it solidifies, usually at constant N and decreasing T. In the case of copper metal, it is not necessary to take care in this type of calculations of the evaporation of atoms effects, because there are very large differences between melting and boiling points; as a result, the evaporative cooling is negligible.

Another model is referred to as a solid state growth model, and it is simulated by adding single atoms to a small initial seed at constant temperature. In photo-curing of copper nanoclusters, it may not be assumed that the temperature is constant, because there is an effect of freezing of liquid nano-droplets.

A good model is to mimic a thermal contact with the surroundings that is cooler. In such a way, one can take into account the most relevant parameters such as the rate of temperature change. Following this approach (see, Westergren, J., H. Gronbeck, A. Rosen, and S. Nordholm, 1998, J. Chem. Phys. 109, 9848), one can obtain that the change in the temperature is inversely proportional to the radius R of the nanocluster:

$$\frac{\partial T}{\partial t} \propto \frac{1}{R} \qquad (6)$$

The growth of copper nanoclusters is dominated by polyicosahedral structures, as mentioned above. It is interesting to note that theoretically it was proven that there are some magic sizes, or values of N, that these polyicosahedral structures prefer, meaning they have the most stability. For example, Figure 4 illustrates the growth process of Cu_{38} at a temperature of 400°K.

Anomalous heat capacity of nanoparticles and the photo-curing process

To understand the photo-curing process, one takes into account the anomalous heat capacity of nanoparticles (see, Likhachev, V.N, et al, Anomalous heat capacity of nanoparticles, Phys. Lett. A 357, 236). The question is why one should expect at all an anomalous heat capacity behavior of nanoclusters or nanoparticles. Under most circumstances, such a heat capacity is qualitatively similar to that of the bulk counterpart. The problem is, however, that in the formation of the nanoclusters or their melting, there is a region of coexistence of two or more phases. This issue can create some peculiar behavior of heat capacity. In the photo-curing process, there is a situation of phase changes of nanoclusters. The thermodynamics of such small systems is outside the range of the regular textbook of thermodynamics.

Refer to the equilibrium for two phases for understanding. The equilibrium between two phases, whether in a bulk form or nanocluster form, can be described by an equilibrium constant:

$$K_{eq}(T) = exp(-\Delta F/KT) \quad (7)$$

whereby ΔF is the free energy difference between the solid and the liquid. However, it is known that:

$$\Delta F = N\Delta\mu \quad (8)$$

And as a result, the equilibrium constant can be expressed as:

$$K_{eq}(T) = exp(-N\Delta\mu/KT) \quad (9)$$

where N is the number of particles in the system, and $\Delta\mu$ is the mean difference in the chemical potentials of the two phases.

Hence, even if $\Delta\mu/KT$ is very small (approximately 10^{-10}), but N is of order of 10^{20}, then the thermodynamically unfavored phase is so unfavored that it is simply unobservable. However, if N is of order of 10 or 1000, then as long as each phase persists long enough to establish conventional properties by which it is recognized as such, it can be quite easy to find ranges of temperatures and pressure in which two or more phases may coexist in thermodynamic equilibrium. Indeed, as discussed above, in the case of copper nanocluster melting or freezing, there may be situations where isomers may coexist, which as a result may induce the anomalous heat capacity behavior. This is taken into account, as well as other variables, when modeling the photonic curing as temperature induced phase transitions in copper nanoclusters. This type of modeling uses extensive molecular dynamics (MD) and jump-walking Monte Carlo (MC) simulations (see, Proykova, A., et al., "Temperature induced phase transformations of molecular nanoclusters," Vacuum, 68 (2003), 87), which needs to treat solid-solid transformation, solid-liquid transformation, and cooling below the solidification point phenomena. This is very complex and uses several millions of configurations and averaging these simulations over different clusters with the same size. This type of calculation and modeling is out of the scope of the photonic curing experimentations.

The complication of the modeling is even more extensive if one takes into account coalescence. The process is so complex that one must consider the

coalescence between two solid clusters, a liquid and a solid cluster and two liquid clusters; while the coalescence of two liquid clusters takes place rapidly, the process of coalescence of two solid clusters takes much longer.

In any case, researchers concluded that coalescence of two solid clusters is very complex, takes place on a very slow time scale and may involve either the formation of a single domain cluster or complicated structures presenting grains (see, Zhu, H., 1996, Philos. Mag. Lett. 73, 27). What exactly happens depends on size and structure of the initial clusters, so it may be a function in photo-curing of the initial size of copper nanoparticles that are used.

Absorption spectra of nanoparticles:

The photo-curing process, involves a study and analyzation of the light absorption by small metal particles. The theory of light absorption by small particles is described by Mie's formulation (see, Mie, G., Ann. Phys. 1908, 25, 377). The absorption spectrum of particles in a given solvent can be calculated from the optical constants of the bulk metal, although the absorption of the particles is recognized to be often vastly different from that of the bulk metal itself. The simplest case is when the particles are spherical and their size is small compared to the wavelength of light. Furthermore, to simplify, assume that the particles are well separated in the solution. Following Mie's theory, at particle sizes between about 3 and 20 nanometers, there is no strong dependence of the absorption spectra on particle size. This is because at this very small particle size, the mean free path of the electrons of the bulk metals is much larger, and as a result, the most significant term in Mie's formula is due to the dipole term, which depends only on the total metal concentration in the solution, not the particle size. In this case, the absorption coefficient in $mol^{-1} \cdot L \cdot cm^{-1}$ is calculated from the relation:

$$\alpha = \frac{18\pi}{In\ 10} \cdot \frac{10^5}{\lambda} \cdot \frac{Mn_0^3}{\rho} \cdot \frac{\varepsilon_2}{(\varepsilon_1 + 2n_0^2)^2 + \varepsilon_2^2} \qquad (10)$$

where:

- λ is the wavelength of light in nm;
- M is the molecular weight;

- ρ is the density of the metal;
- n_0 is the refractive index of the solvent; and
- ε_1, ε_2 are the real and the imaginary parts of the dielectric constant of the metal.

An interesting situation is when the size of the particles becomes smaller than the mean free path of the electrons (for silver, 52 nanometers, and for copper, 39 nanometers). In this case, the absorption bands are broadened. The reason is that a size correction is necessary, and the formula equation (10) starts to be size-dependant (see Kreibig, U., J. Phys. F 1974, 4, 999), because

$$\varepsilon_2 = \varepsilon_{2(bulk)} + (\omega_p^2/\omega^3)(v_F/R) \qquad (11)$$

where:

- ω is the light frequency;
- ω_p is the plasmon frequency of the specific metal;
- v_F is the electron velocity at the Fermi level; and
- R is the particle radius.

Basically, the ratio R/v_F is the mean time of the free movement of the electrons in the specific metal particle.

Extensive modeling and calculations using Mie's formulation were done by Creighton and Eadon (see, Creightoin, J.A., Eadon, D.G. J. Chem. Soc., Faraday Trans. 1991, 87, 3881) (see Figure 5). Figure 5 shows, taking into account dipole approximation, a situation that explains well the absorption of metals below a wavelength of 400 nanometers. In order to complete the entire picture of the absorption, one needs to take into account the electronic energy levels and the allowed optical transitions in the specific metal. First of all, one needs to treat the intraband transitions, which in some cases require the participation of a phonon. If this is the case, these intraband transitions will not significantly contribute to the absorption of light. However, an intense absorption is observed in some metallic particles, which peaks at a lower photon energy that is produced by a collective excitation of the free electrons in the particles, as it is illustrated in Figure 6.

Referring to Figure 6, the movement of the electrons under the influence of the electric field vector of the incoming light leads to a dipole excitation across the particle sphere. The positive polarization charge then is acting as a restoring force which makes the electrons oscillate. Thus, the electron density within a surface layer of a few angstroms (which is about equal to the screening length) oscillates, while the interior of the particle remains constant. It is important to note that in some cases (such as silver), the excitation of the collective oscillations (plasmon absorption) and the intraband transitions occur at separated wavelength regimes. In the case of copper (as well as gold), the plasmon resonances occur in the visible. However, these resonances are superimposed by intraband transitions.

The contribution of the plasmon oscillation to the absorption of a metal particle can be treated separately. For example, the Mie's equation for the absorption constant is then described as:

$$K = 9\pi NVn_0^3 c\lambda^2/\sigma[(\lambda_m^2 - \lambda^2)^2 + \lambda^2\lambda_m^4/\lambda_a^2] \quad (12)$$

where

- K is the absorption constant in cm^{-1}, $K = \alpha\, c\, \ln 10$, whereby c is the concentration of the metal in moles/liter;
- N is the particle concentration;
- V is the volume per particle;
- $\lambda_m^2 = \lambda_c^2(\varepsilon_0 + 2n_0^2)$ is the wavelength of maximum absorption;
- ε_0 is the high frequency dielectric constant of the metal;
- λ_c is the plasma wavelength, $\lambda_c^2 = (2\pi c)^2 m/4\pi N_e e^2$, and is a typical metal property;
- N_e is the density of the free electrons;
- λ_a is constant related to the bandwidth at half maximum absorption, $\lambda_m^2/\lambda_a = (\varepsilon_0 + 2n_0^2)c/2\sigma$;
- σ is the DC conductivity, $\sigma = N_e e^2 \{r\}/mv_F$;
- M is the effective electron mass;
- $\{r\}$ is mean free path of the electrons in the colloid;

- $1/\{r\} = (1/r + 1/r_\infty)$; and
- r_∞ is the mean free path in the bulk metal.

The relations above indicate that the band position does not depend on the size of the particles. An increase in N_e by adding electrons to the particles' surfaces should lead to a blue shift and a decrease in bandwidth, and consequently, to an increase in the absorption maximum.

Nanoparticles agglomeration effects on the absorption spectra:

A good comparison between experiment and calculations of observed spectra has been previously possible for a limited number of cases. The main reason is that the metal often does not form isolated particles in colloidal solutions, but agglomerates of a few or even a large number of particles. The agglomeration can drastically change the absorption spectrum. Typical examples are shown in Figure 7 where absorption spectrums of cadmium and thallium colloids are graphed.

Spectra (a) in Figure 7 were obtained for solutions which contain agglomerated particles, while Spectra (b) were obtained for solutions prepared under conditions where agglomeration did not occur. Spectra (b) is in good agreement with Mie's formulation and also with the calculated spectrum in Figure 5.

In view of the description above and the results in Figure 7, a colloidal metallic substance appears black if the spectrum is similar to the Spectra (a). On the other hand, if the particles are not agglomerated (i.e., good dispersion and good isolation between particles), observed is a more metallic-like color, indicated by Spectra (b).

As summarized in Figure 8, there is a resulting correlation between average particle size, the powder color, the ink color and the resistivity after curing. Good inks are produced when the color of the powder and the inks are in the red-brown or brown range. When there are very black or very dark looking particles and inks, there is agglomeration.

As the solution is aging, there is a dynamic change of the absorption spectrum from Spectra (b) to Spectra (a) (see Figure 7). The reason is that at the initial stage there are well-dispersed and isolated copper nanoparticles, while due to the aging process, there will be larger and larger agglomerations. As a result, the color of the

copper colloid changes from a metallic red-brownish color to a darker color, eventually transitioning to black.

A very interesting experiment is described (see, Henglein, A., J. Phys. Chem. 1993, 97, 5457-5471) in the spectrum of an aged cadmium (Cd) solution. The aged cadmium solution was exposed to nitrous oxide and then the spectrum was measured as a function of time. The cadmium particles slowly react with N_2O according to the following equation:

$$Cd^0 + N_2O + H_2O \rightarrow Cd^{++} + N_2 + 2OH^- \qquad (13)$$

As can be seen in Figure 9, not only the intensity of the absorption decreases during this reaction, but also the shape of the spectrum, with the long wavelength peak rapidly disappearing. The effect is attributed to a phenomenon that occurs frequently in redox reactions of agglomerated colloids color; the agglomerates disintegrated to yield more or less isolated particles. This is attributed to charging of the particles: as the reaction with N_2O is progressing, the particles become positively charged and repel each other.

Copper oxide to copper reduction during the photo-curing process:

Copper nanoparticles (~50 nm) from Sangyo and American Elements (80 nm) are formulated with B1-type ink (IPA, Hexylamie and copper nanoparticles). Both sets of copper nanoparticles contain copper oxides over 20%. Evidence shown in Figure 10 indicates that photonic curing can photo-reduce copper oxides to metallic copper.

With a flash lamp, a threshold energy may exist for photo-reduction of copper oxides. Respective XRDs of the photo-cured inks were executed for both Sangyo and American Elements B1 type ink formulations. Figure 11(a) shows the Sangyo copper nanoparticles XRD after precuring at 100°C in air; observed in Figure 11(b) are the changes to the XRD after the photonic curing process.

In this case, Cu_2O was completely transformed to copper (200). The same phenomena was observed with American Elements copper nanoparticles, but in this case dependency on the voltage of the photo-curing lamp was observed (see Figure 12). Figure 12A illustrates American Elements copper nanoparticles pre-cured at 100°C in air; Figure 12B illustrates American Elements copper nanoparticles are photonic-cured at a voltage of 1300 V and bluish color is observed after photonic

curing; Figure 12C illustrates American Elements copper nanoparticles are photonic-cured at a voltage of 1400 V and reddish color is observed after photonic curing.

The visual and XRD data indicate that the reduction of copper oxide to metallic copper is occurring during photonic curing. Following the work of Fleisch (T. H. Fleisch, et al., J. App. Surf. Sci., 10, 50 (1982)), when the band gap of the metal oxide is greater than the enthalpy of formation of the metal oxide, photo-reduction to metal can be achieved by radiating the metal oxides having energy higher than the band gap. The band gaps for Cu_2O and CuO are 1.9 eV (188 kJ/mol) and 2.6 eV (257 kJ/mol), respectively. The corresponding enthalpies of formation of Cu_2O and CuO are 157 kJ/mol and 168 kJ/mol, respectively. Thus, the UV radiation from 100 nm to 400 nm reduces copper oxide to metallic copper.

Nanoparticles optical absorption spectra and the flash lamp spectral distribution:

Based on the analysis of the optical absorption spectrum, the spectral distribution of the flash lamp is important. The spectral distribution illustrated in Figure 13 is typical of a xenon lamp whereby approximately 6% of the power used is emitted in the form of UV radiation below 380 nm. Most of the photonic energy actually ranges from visible to infrared wavelengths. It may be useful to have the UV lamp with a higher energy density in UV range as compared with the current flash lamp.

Another possible UV lamp containing decaying excimer complexes may provide improved photonic curing lamps that can fuse and photo-reduce copper oxides at the same time. Excimer lamps offer high intensity narrow band radiation at various UV and VUV wavelengths. Excimer lamps can be extremely efficient energy converters transforming electron kinetic energy into UV radiation. No self-absorption is observed in excimer systems. In most cases, excimer forming gas mixtures exhibit one dominant narrow emission band. Excimer systems can be pumped at extremely high power densities before saturation effects start to limit the spontaneous emission. Thus, extremely bright UV and VUV sources can be built and used with embodiments of the present invention.

This analysis also explains results with the Optomec printer, and may direct even further to a better choice or laser mono-chromatic radiation for achieving the best curing results.

As noted previously, in a process to photosinter metallic inks, they are pre-dried to remove excess vehicles and solvents. This can be carried out in air including with the aid of an oven, but this may require 30 – 60 minutes of drying time. In a manufacturing process, this time may be too long. The following alternative embodiment describes methods of reducing this drying time.

Referring to Figure 26A, a device 800 is shown for simultaneous or near-simultaneous inkjetting and photo-curing of nanoparticle copper films (or any other suitable metal ink). The device includes an inkjet dispenser 802 for dispensing copper ink 801 onto the surface of a substrate 804. The device 800 also includes a light source 806 for curing the ink films 803 deposited by the inkjet dispenser 802. The light source can be a laser source (pulsed or continuous), a pulsed lamp, or a focused beam. In some implementations, the dispenser 802 is arranged to automatically pass over the substrate along a predetermined pathway. Additionally, the dispenser 802 can be arranged to dispense the copper ink at multiple predetermined positions and times above the substrate 804. The light source 806 can be attached to the inkjet dispenser 802 or arranged to travel over the substrate 800 separately from the dispenser 802. The light source 806 can be arranged to photo-cure the inkjetted films immediately after they are deposited by the dispenser 802. Alternatively, the light source 806 can be arranged to photo-cure the films at predetermined times following the deposition of the film. The motion of the light source 806 and the dispenser 802 can be controlled by a computer system/controller arrangement 808. A user may program the computer 808 such that the controller automatically translates the dispenser 802 and light source 806 over a predetermined path. In some implementations, the light source 806 and dispenser 802 are fixed and the substrate is placed on a movable platform controlled by the computer/controller 808.

A flow chart of a photo-curing process is shown in Figure 26B. A solution of metal ink is mixed (810) and then printed or dispensed (812) onto the substrate 804 using the dispenser 802. The film deposition is tightly controlled so a well-defined pattern is formed. The film then is dried (814) to eliminate water or solvents.

In some cases, a thermal curing step can be introduced subsequent to dispensing the film and prior to the photo-curing step. The substrate and deposited film can be cured using an oven or by placing the substrate on the surface of a heater, such as a hot plate. For example, in some implementations, the film is pre-cured in

air at 100°C for 30 minutes before photo-curing. Alternatively, the thermal curing can be performed by directing a laser onto the surface of the film. Following the drying and/or thermal curing step, a laser beam or focused light from the light source 806 is directed (816) onto the surface of the film in a process known as direct writing. The light serves to photo-cure the film such that it has low resistivity. Generally, the metal films are insulating after the printing/dispensing and drying steps. After the photo-curing process, however, the insulating film becomes a conductive film 809 (see Figure 26A).

In some implementations, the dispenser 802 is used to deposit a blanket film or a coarse outline of the pattern. Typically, printing techniques can achieve feature sizes on the order of 25 – 50 microns or greater. If finer features are necessary, the pattern/blanket film can be refined or reduced using a focused beam of light or laser, in which case the features are defined by the spot size of the laser or by the focus of the light beam. Typically, light can be focused to 1 micron or less. Thus, submicron features may be possible. Ultimately, the feature size may be limited by the size of the nanoparticles used in the conductive film. Metal particles can be formed to have features on the order of 1 - 5 nm.

Effect of vacuum drying on copper nanoparticle inks:

An experiment was performed to determine the effect of drying the copper nanoparticle inks in a vacuum environment as opposed to an airflow environment. The sample was prepared by sonication and hand agitation. The samples were then printed and dried. Then a vacuum oven was used to dry the inks at various temperatures. For comparison, baseline samples were also prepared in an airflow environment at atmosphere. All samples were photosintered, and the electrical and adhesive properties were measured. A result is that the drying time for the selected ink is significantly reduced if the drying takes place in a vacuum environment.

Processes above describe copper ink samples dried in an airflow environment at atmospheric pressure for 30 – 60 minutes, depending upon the formulation of the ink. This drying is performed in order to remove by evaporation the solvents that remain in the ink after printing. Evaporation of the solvents aids in the photosintering process that follows. If the ink contains excessive amounts of solvent, the result is what is referred to as “blowoff,” a condition where the solvent evaporates rapidly, in

fact almost instantly, causing the copper nanoparticles to be blasted off of the substrate and into the surrounding environment.

By removing the solvents more rapidly, the process can be more cost effective for a high-throughput manufacturing system. Experiments were performed at various temperatures but at one vacuum level. It was found that the drying time for a selected ink is reduced when dried at 100°C or 125°C without significantly affecting the conductive or adhesive properties when compared to the baseline samples dried in an airflow environment. At 150°C, however, the conductive properties tend to diminish. While the data collected from this experiment proves that drying times are shortened through vacuum drying, this process may also be expanded to include lower temperatures and shorter drying times to further enhance the viability of copper inks in a mass production scenario.

The formulated ink was then sonicated and hand agitated to break up any agglomerations. It was used in a shelf life study for several weeks and then was stored on a shelf until this experiment. Prior to draw-down printing, the ink was hand agitated for approximately 30 seconds, sonicated for 16 minutes, and hand agitated for an additional 30 seconds.

Methods Used:

Draw-Down Printing

Printing was accomplished using a draw-down printer on a Kapton substrate using a #10 wire-wrapped rod. The rod was coated in ink and then drawn across the surface to provide an even coating. Several samples were printed in the same manner to accommodate the scope of the experiment. After printing, the samples were allowed to air dry on a shelf.

Airflow Drying

Two samples were dried in an airflow oven at 100°C, one for 30 minutes and one for 60 minutes. These samples were made to provide a baseline of a standard procedure for later comparison to the vacuum dried samples.

Vacuum Drying

The remaining samples were dried in a vacuum oven at various temperatures and for various lengths of time. Figure 14 shows the drying parameters for each sample. After heating and pumping the empty vacuum oven for outgassing and

removing contaminants, the oven was then vented and the following procedure was used for each sample:

- Check and record platform temperature by an infrared (IR) thermometer
- Place the sample in the center of the platform
- Begin vacuum pumping
- When pressure reaches approximately -25 inches Hg (93 seconds on average), start the timer
- When time has expired, record oven pressure (approximately -29.5 inches Hg for all samples)
- Immediately vent the oven
- When the oven is vented, check and record platform temperature with the IR thermometer
- Repeat for all samples

Presintering Preparation

Upon completion of the airflow and vacuum drying, all samples were then scored to provide an adhesion test pattern. The samples were also numbered and measured on a profilometer to provide thickness data before the photosintering step.

Photosintering

Photosintering is the previously described method used to cure the inks to a conductive copper film. This involves exposing the ink to a short pulse of highly concentrated UV light. All samples were photosintered using the same power and pulse widths for each shot. The power used was 1200 V and the pulse widths were 400, 500, 600, 700, and 800 microseconds.

Properties Testing

After photosintering was complete, the adhesive and electrical properties of each sample were characterized. First, sheet resistance of the film was measured using a 4-point probe method. Second, the film thickness was measured on the profilometer. Finally, the adhesion was tested using the ASTM Standard Test Method for Measuring Adhesion by Tape Test. After all data were collected, the resistivity was calculated using the sheet resistance and thickness data.

Results

Referring to Figure 15, the electrical properties for samples 3 - 8 are very similar to that of sample 2, which was processed using a standard thermal procedure

for this formulation. However, samples 9 and 10, which were dried at 150°C under vacuum significantly increased resistivity. Adhesion was excellent (10 on a scale of 1 - 10) for all samples in this experiment. These data indicate that vacuum drying is a viable solution to shortening the drying time of copper nanoparticle inks. Figure 16 shows the percentage blowoff of the copper from the Kapton during the photosintering step. These results show that resistivities in the micro-ohm-cm range with excellent adhesion are achieved in vacuum, and that comparable resistivities are obtained with vacuum drying for 5 minutes at 125°C (sample # 6) as compared to drying at 1 atmosphere pressure for 60 or 30 minutes at 100°C. Sample # 6 has only 5% copper blowoff.

Effect of infrared drying on copper nanoparticle inks:

An experiment was performed to determine the effect of drying copper nanoparticle inks under an infrared lamp as opposed to an airflow oven environment (standard drying process). The sample was prepared by sonication and hand agitation. The samples were then printed and air dried. An infrared lamp was then used at various distances to further dry the inks. For comparison, one sample was cured with no drying process and another sample was dried in an airflow oven environment. All samples were photosintered, and electrical and adhesive properties were measured. The data collected in this experiment indicates that drying by infrared lamp reduces the drying time required when compared to airflow oven drying. Interestingly, the sample that was not subjected to any drying process showed similar electrical properties to the sample that was dried in an airflow oven.

The experiment was performed using a commercially available infrared lamp to dry the samples at various distances to the lamp in open air. It was found that drying the sample at a short distance for any reasonable length of time as well as a medium distance for an extended length of time caused significant damage to the ink and in turn caused the ink to blow off during photosintering. Samples dried at medium to long distances for any length of time showed little change and, in some cases, slight improvement when compared with the sample dried in an airflow oven.

While the data collected from this experiment is sufficient in showing that drying times are shortened through infrared drying, this experiment can also be expanded to include a greater variety of parameters (distance and time) to further enhance the viability of copper inks in a mass production setting.

Materials used in this experiment:

Infrared Lamp = Phillips 250W red heat lamp mounted in a clamp-on style reflector socket

Airflow Oven = Despatch (model #LCCL-54)

Draw-Down = Gardco Auto-Draw III (model #DP-1250)

Solid copper nanoparticles were added to the dispersion medium in an N_2 purged glove box, and the chunks were broken up in the media with a small spatula. The ink was then sonicated and hand agitated to break up any agglomerations. It was used in a shelf-life study for several weeks and then was stored on a shelf. Just prior to draw-down printing, the ink was hand agitated for approximately 30 seconds, sonicated for 8 minutes, and hand agitated for an additional 30 seconds.

Methods Used:

Draw-Down Printing

Printing was accomplished using a draw-down printer on a Kapton substrate using a #10 wire-wrapped rod. The rod was coated in ink and then drawn across the surface to provide an even coating. Several samples were printed in the same manner to accommodate the scope of the experiment. After printing, the samples were allowed to air dry on a shelf. One sample was left in this state before curing.

Airflow Baking

One sample was dried in an airflow oven at 100°C for 30 minutes. This sample was made to provide a baseline of a standard recipe for later comparison to the infrared dried samples.

Infrared Drying

The remaining samples were dried under an infrared lamp at various distances to the lamp and for various lengths of time. Figure 17 shows the drying parameters for each sample. The samples were dried on an insulating ceramic platform to minimize heat transfer from the sample to the platform and vice-versa.

Pre-Sintering Preparation

Upon completion of sample drying, all samples were scored to provide a means of measuring film thickness. The samples were then measured on a profilometer to provide thickness data before the photosintering step.

Photosintering

All samples were photosintered using the same power and pulse widths for each shot. The power used was 1200 V and the pulse widths were 500, 600, and 700

μsec. This an abbreviated version of the standard recipe used at the time of the experiment.

Properties Testing

After photosintering was complete, the adhesive and electrical properties of each sample were characterized. First, sheet resistance of the film was measured using a 4-point probe method. Second, the film thickness was measured on the profilometer. Finally, the adhesion was tested by applying and subsequently removing a strip of adhesive tape. After all data was collected, the resistivity was calculated using the sheet resistance and thickness results.

Results

Referring to Figure 18, the electrical properties for samples 5 and 7 – 10 are better than that of sample 2, which was processed using the standard bake for this formulation. However, samples 3 and 4, which were dried at close range, infinite resistivity due to the film being completely blown off during the curing process. Sample 6, which was dried at 6 inches for 30 minutes, also possessed increased resistivity. Adhesion was acceptable for most samples in this experiment. Blowoff was an issue on virtually all samples ranging anywhere from 10% to 100% depending upon the drying parameters. Sample 1 was only dried in air with no applied heat. This sample, while exhibiting slightly more blowoff, had a comparable resistivity to the oven dried sample. Overall, this data indicates that while infrared drying reduces the drying time required as well as the resistivity, blowoff may be an issue. Figure 19 shows the percentage blowoff of the copper from the Kapton during the photosintering step.

Conclusions

Sample #14 had a low resisitivity of 6.24 microohm-cm with a small blow off (30%) of the copper conductor (see Figures 18 and 19).

Effect of microwave drying:

Solvent based inks

An experiment was performed to determine the effect of microwave drying of copper nanoparticle inks as opposed to airflow oven drying. The sample was prepared by sonication and hand agitation. The samples were then printed and dried. Then a microwave oven was used to dry the inks for various periods of time. For comparison, a baseline sample was also prepared in an airflow oven environment. Finally, all samples were photosintered and electrical and adhesive properties were

measured. The data collected in this experiment indicates that microwave drying of copper nanoparticle inks provides no significant increase in ink performance.

The experiment was performed for various periods of time, but at only one power level (100%). It was found that the drying time for the selected ink may not be reduced by microwave drying when compared to the baseline samples baked in an airflow oven. While the data collected from this experiment is believed to be sufficient in proving that drying times may be unaffected by microwave drying, this experiment may also be expanded to include different power levels and longer drying times to further enhance the data.

Materials used:

Microwave Oven = General Electric Household Microwave Oven (model #JES737WM01)

Airflow Oven = Despatch (model #LCCL-54)

Draw-Down = Gardco Auto-Draw III (model #DP-1250)

Ink formulated:

Solid copper nanoparticles were added to the dispersion medium in an N_2 purged glove box and chunks were broken up in the media with a small spatula. The ink was then sonicated and hand agitated to break up any agglomerations. It was used in a shelf life study for several weeks and then was stored on a shelf until this experiment. Prior to draw-down printing, the ink was hand agitated for approximately 30 seconds, sonicated for 8 minutes and hand agitated for an additional 30 seconds.

Methods Used:

Draw-Down Printing

Printing was accomplished using a draw-down printer on a Kapton substrate using a #10 wire-wrapped rod. The rod was coated in ink and then drawn across the surface to provide an even coating. Several samples were printed in the same manner to accommodate the scope of the experiment. After printing, the samples were allowed to air dry on a shelf.

Airflow Baking

One sample was baked in an airflow oven at 100°C for 60 minutes. These samples were made to provide a baseline of the standard recipe for later comparison to the vacuum baked samples.

Vacuum Baking

The remaining samples were dried in a microwave oven for various periods of time. Figure 20 shows the drying parameters for each sample. Each sample was placed in the center of the microwave on the rotating glass plate.

Pre-Sintering Preparation

Upon completion of the airflow and microwave drying, all samples were scored and measured on a profilometer to provide thickness data before the photosintering step.

Properties Testing

After photosintering was complete, the adhesive and electrical properties of each sample were characterized. First, sheet resistance of the film was measured using a 4-point probe method. Second, the film thickness was measured on the profilometer. Finally, the adhesion was tested by applying and subsequently removing a strip of adhesive tape. After all data was collected, the resistivity was calculated using the sheet resistance and thickness data.

Results

Referring to Figure 21, shows that samples 2 - 5 had increased resistivity when compared to that of sample 1, which was processed using the standard bake for this formulation. Blowoff may be an issue with all samples ranging anywhere from 10% to 80% (see Figure 22). Adhesion was marginal at best (3 to 8 on a 10 point scale) for all samples. This data indicates that microwave drying may not be a viable solution to shortening the drying time of copper nanoparticle inks.

Conclusions

Samples 3 and 4 low resistivity while having only 20% blowoff during photosintering (see Figure 22).

Water based inks

The ink was a water-based copper ink. The data in Figure 23 shows the electrical properties for the samples in Figure 24. The post-sintering thickness for sample 1 is in question, hence the unrealistically low resistivity.

Figure 25 shows the percentage blowoff of the copper from the Kapton during the photosintering step.

Conclusions

These results show that drying the coated samples from the water based inks using 30 seconds of microwave radiation may provide a low resistivity (see Figure 23) while keeping the blowoff to only 10% (sample 2) (see Figure 25).

These results show that resistivities in the micro-ohm-cm range with excellent adhesion are achieved in vacuum, and that comparable resistivities are obtained with vacuum drying for 5 minutes at 125°C as compared to drying at 1 atmosphere pressure for 60 or 30 minutes at 100°C.

A number of embodiments of the invention have been described. Nevertheless, it will be understood that various modifications may be made without departing from the spirit and scope of the invention. For example, other conductive metals may be used instead of, or in addition to, copper.

Summary

In summary, optical absorption of copper inks is a complicated system of many particles, which is determined by both properties of the individual structural units and the collective effects due to the interaction among particles. This spectrum often contains both the plasmon band of the single particles and sometimes more maxima attributed to excitation with the electric field parallel (low energy mode) and normal (high energy mode) to the axes of a chain of agglomerated particles. In this case, approximation of the metallic particle to a spherical shape is not accurate anymore, and one needs to look at a prolate spheroidal as the calculations were made in Figure 5. Indeed, observed from Figure 5 is that as the agglomerates become more ellipsoid-like, the spectrum is changing from Spectra (b) to Spectra (a), as discussed above.

Determined:

(A) The color and the size distribution of the metallic copper nanoparticles in a dry form or in a solution;

(B) The mean free path of electrons in bulk copper is 39 nanometers explains the empirical choice of particles around 50 nanometers whereby the size of the particles, if well-dispersed, is of the same magnitude as the electron mean free path;

(C) The heat capacity behavior of nanoparticles as a function of size and why during the photo-curing process fusion and excellent electrical conductivity results are obtained;

(D) The optical behavior of copper metallic nanoparticles and correlation of the color of the ink with good dispersion qualities and eventually better fusion in the photo-curing process;

(E) The transformation of the copper oxide to copper during the curing process with direct relations to the ink quality and the resistivity after the photonic curing process;

(F) An optimal lamp for photo-curing. Having a lot of energy in the visible and in the infrared ranges may not be useful. A good dispersion of isolated copper nanoparticles may require energies with a wavelength lower than 400 nanometers. This may simplify the availability of suitable lamps and lower their energy consumption.

(G) Certain photo-curing processes require higher energy for achieving a complete transformation of copper oxide to copper, which provides parameters for an optimal design of the lamps by exploiting the most useful spectrum of the lamp in correlation with the specific copper metallic nanoparticle's manufacturer and the copper nanoparticle size distribution in the ink.

(H) Since the rapid evaporation of volatile components from the ink leads to removal of the metal conductor from the substrate, it is advantageous that they are evaporated prior to the photo-curing step.

(I) Conventional evaporation involves heating in air for 30 or 60 minutes, which can be shortened by using vacuum or microwave drying methods.

We claim:

1. A method comprising:

depositing a pattern of conductive ink comprising clusters of conductive nanoparticles; and

photosintering the conductive ink.

2. The method of claim 1, further comprising drying the conductive ink between the depositing and photosintering steps.

3. The method of claim 2, wherein the drying is performed in a vacuum chamber.

4. The method of claim 2, wherein the drying is performed by an artificial infrared heater.

5. The method of claim 2, wherein the drying is performed with microwave energy.

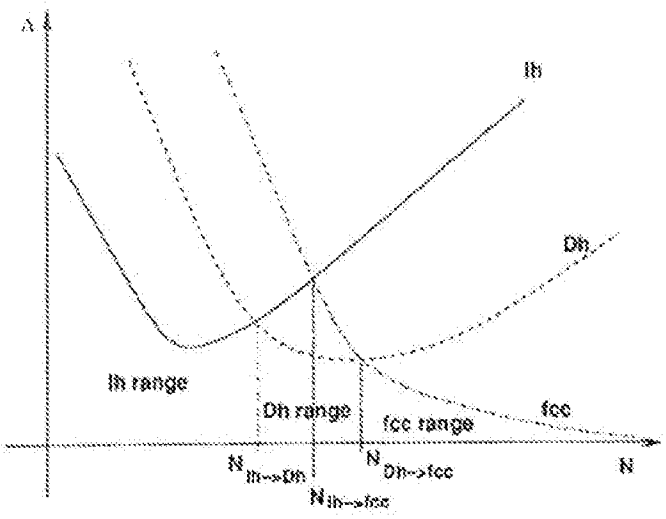
Δ
Ih
Dh
fcc
Ih range
Dh range
fcc range
N
N Ih->Dh
N Dh->fcc
N Ih->fcc

FIG. 1

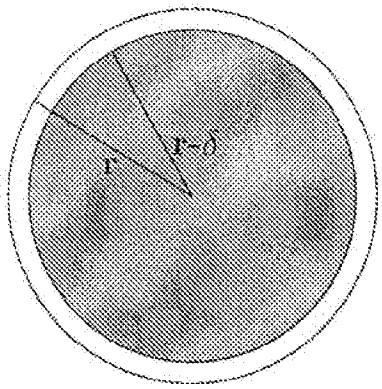
r=0

FIG. 2

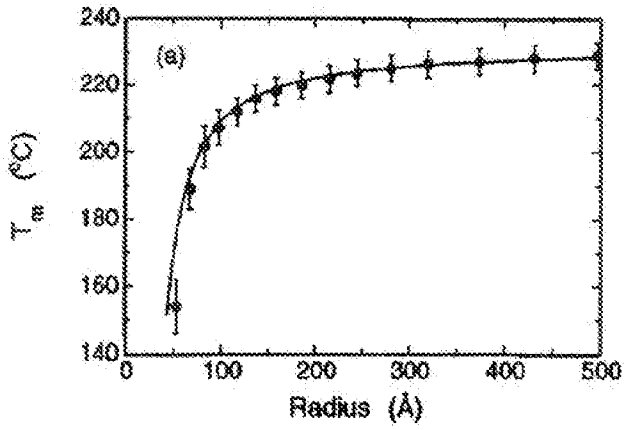
(a)
240
220
200
180
160
140
0
100
200
300
400
500
Radius (Å)
T_e (°C)

FIG. 3

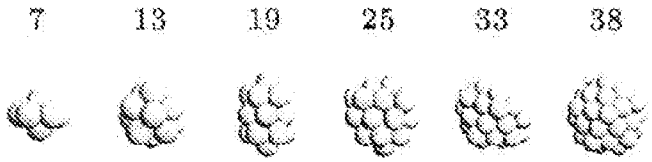
7
13
19
25
33
38

FIG. 4

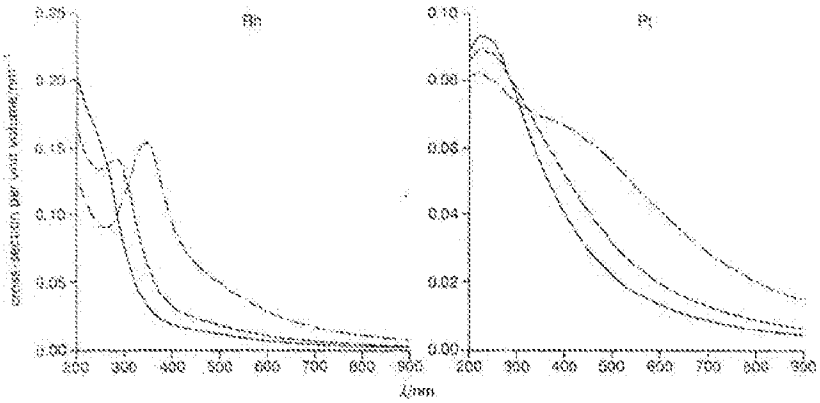
0.25
0.20
0.15
0.10
0.05
0.00
200
300
400
500
600
700
800
900
0.10
0.08
0.06
0.04
0.02
0.00

FIG. 5

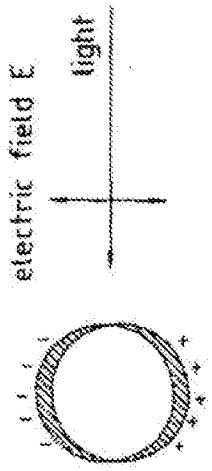
electric field E
light

FIG. 6

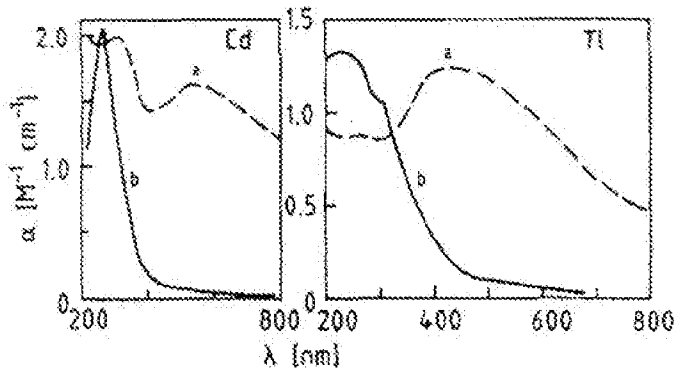
Cd
Tl
a
b
2.0
1.0
0
1.5
1.0
0.5
0
200
800
200
400
600
800
λ (nm)

FIG. 7

Item	Manufacturer	Particle size-AVG (nm)	Powder color	Ink color	Best resistivity (μohm-cm)
1	Alfa Aesar	40	black	black	144
2	Aldrich	90	red brown	red brown	32
3	Novacentrix	50	red brown	red brown	92
4	Junye	80	black	black	480
5	Junye	110	red brown	red brown	15
6	Junye	80	brown	brown	7
7	Junye	60	dark brown	dark brown	86
8	Junye	70	brown	brown	5
9	American elements	70	dark brown	dark brown	28
10	Ferro	120	red brown	red brown	6
11	Canano	50	dark dark brown	dark dark brown	150
12	Canano	70	dark brown	dark brown	23
13	Canano	90	brown	brown	15

FIG. 8

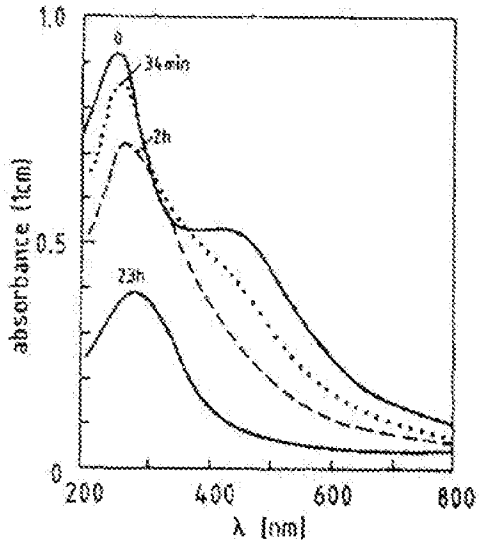

FIG. 9

Copper Nanoparticles (NPs)	Solution		Cu /Cu_2O (Net Height from XRD data)
50 nm Sangyo	IPA, Hexylamine and NPs	Pre-cure At 100°C in air	2.1 : 1
		After photonic curing	13 : 1
80 nm American Elements	IPA, Hexylamine and NPs	Pre-cure At 100°C in air	2.6 : 1
		After photonic curing (Reddish Zones ~1400 V)	3.6 : 1
		After photonic curing (Bluish zone ~1300 V)	2.2 : 1

FIG. 10

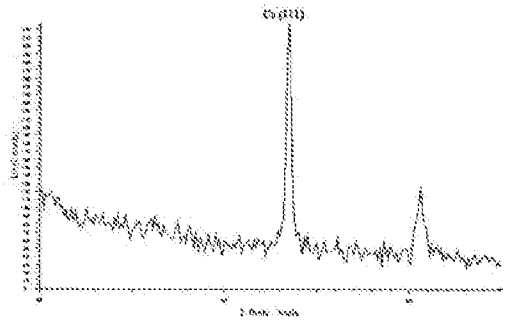

FIG. 11A

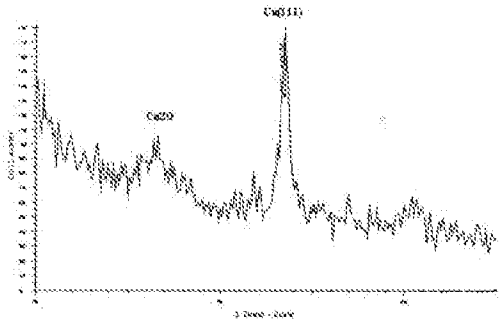

FIG. 11B

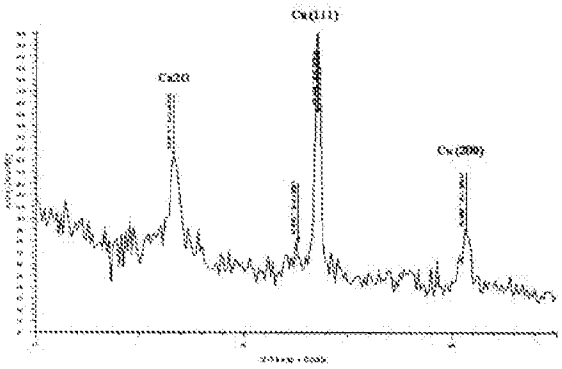

FIG. 12A

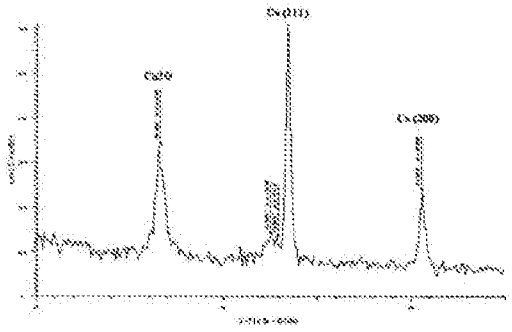

FIG. 12B

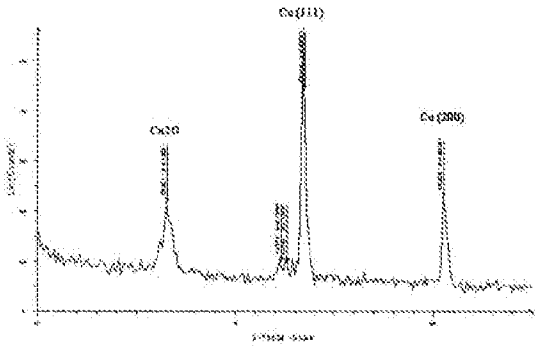

FIG. 12C

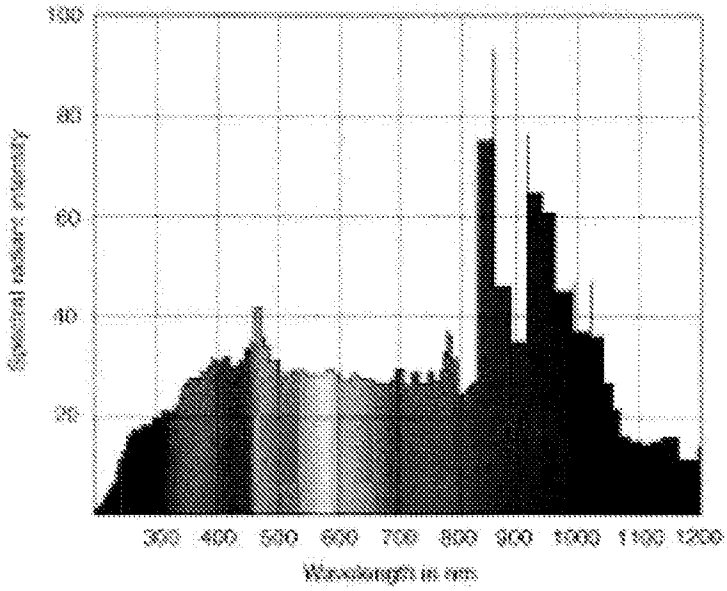

FIG. 13

Sample #	Oven	Drying Time (min.)	Pre Temp (°C)	Post Temp (°C)
1	Airflow	30	100*	100*
2	Airflow	60	100*	100*
3	Vacuum	10	93	93
4	Vacuum	15	93	95
5	Vacuum	20	95	93
6	Vacuum	5	125	121
7	Vacuum	10	121	126
8	Vacuum	15	126	120
9	Vacuum	5	152	145
10	Vacuum	10	145	150

*These values were not verified by an IR thermometer

FIG. 14

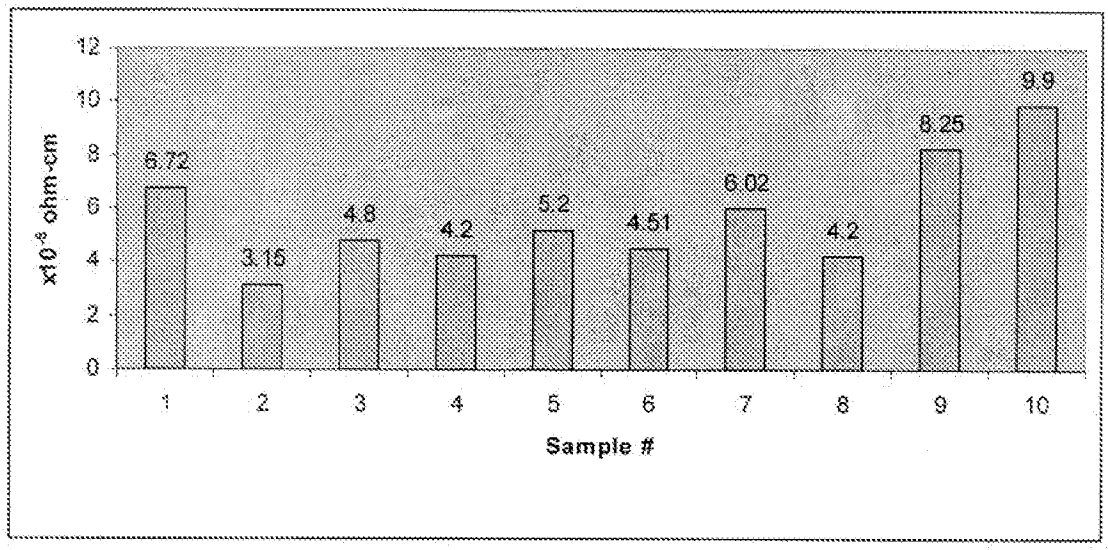
x10⁻³ ohm-cm
0
2
4
6
8
10
12
6.72
3.15
4.8
4.2
5.2
4.51
6.02
4.2
8.25
9.9
1
2
3
4
5
6
7
8
9
10
Sample #

FIG. 15

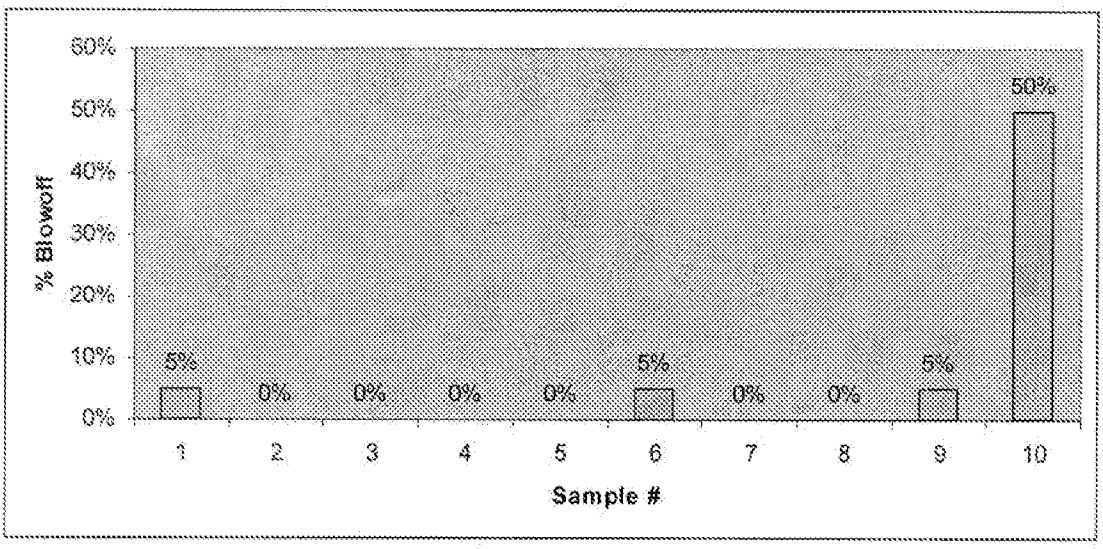
% Blowoff
0%
10%
20%
30%
40%
50%
60%
5%
0%
0%
0%
0%
5%
0%
0%
5%
50%
1
2
3
4
5
6
7
8
9
10
Sample #

FIG. 16

Sample #	Drying Method	Drying Time (min.)	Distance to Lamp (in.)
1	Air	N/A	N/A
2	Airflow Oven	60	N/A
3	Infrared Lamp	1	2
4	Infrared Lamp	5	2
5	Infrared Lamp	15	6
6	Infrared Lamp	30	6
7	Infrared Lamp	15	9
8	Infrared Lamp	30	9
9	Infrared Lamp	15	12
10	Infrared Lamp	30	12

FIG. 17

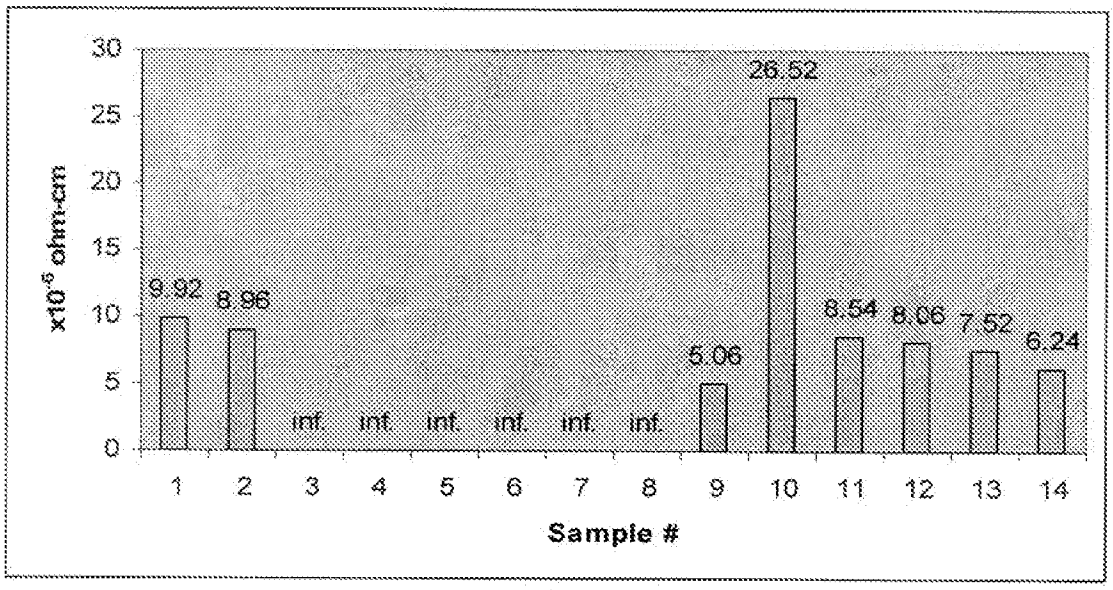
30
25
20
15
10
5
0
x10⁻⁶ ohm-cm
9.92
8.96
inf.
inf.
inf.
inf.
inf.
inf.
5.06
26.52
8.54
8.06
7.52
6.24
1
2
3
4
5
6
7
8
9
10
11
12
13
14
Sample #

FIG. 18

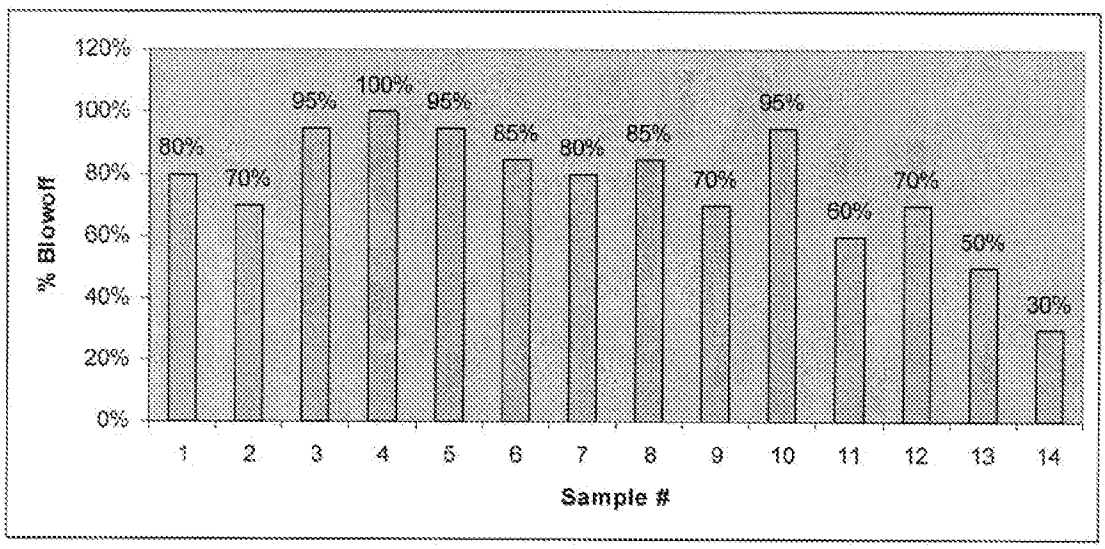
120%
100%
80%
60%
40%
20%
0%
% Blowoff
80%
70%
95%
100%
95%
85%
80%
85%
70%
95%
60%
70%
50%
30%
1
2
3
4
5
6
7
8
9
10
11
12
13
14
Sample #

FIG. 19

Sample #	Oven	Bake Time (min.)	Power level
1	Airflow	60	N/A
2	Microwave	0.5	100%
3	Microwave	1	100%
4	Microwave	2	100%
5	Microwave	4	100%

FIG. 20

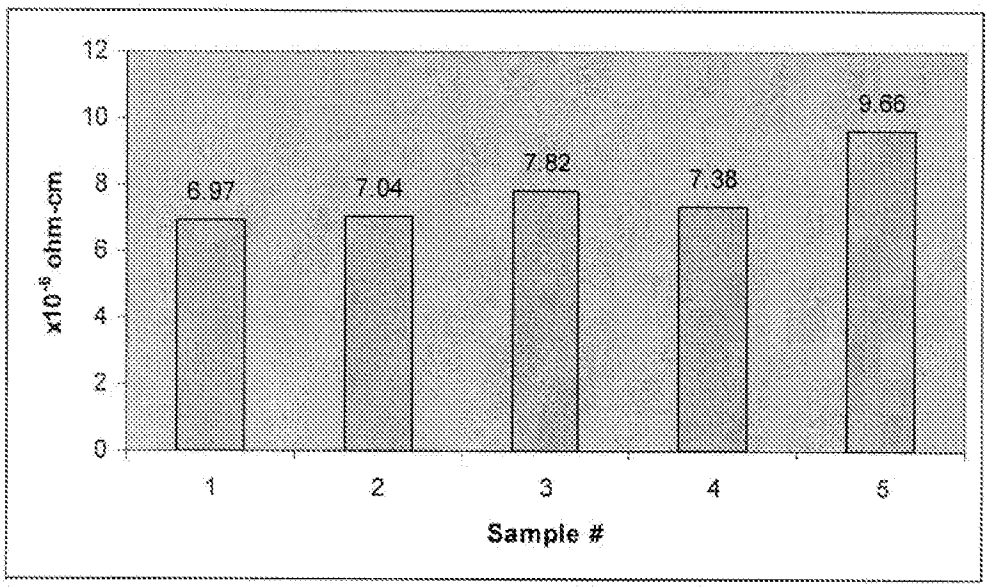
12
10
8
6
4
2
0
x10⁻⁶ ohm-cm
6.97
7.04
7.82
7.38
9.66
1
2
3
4
5
Sample #

FIG. 21

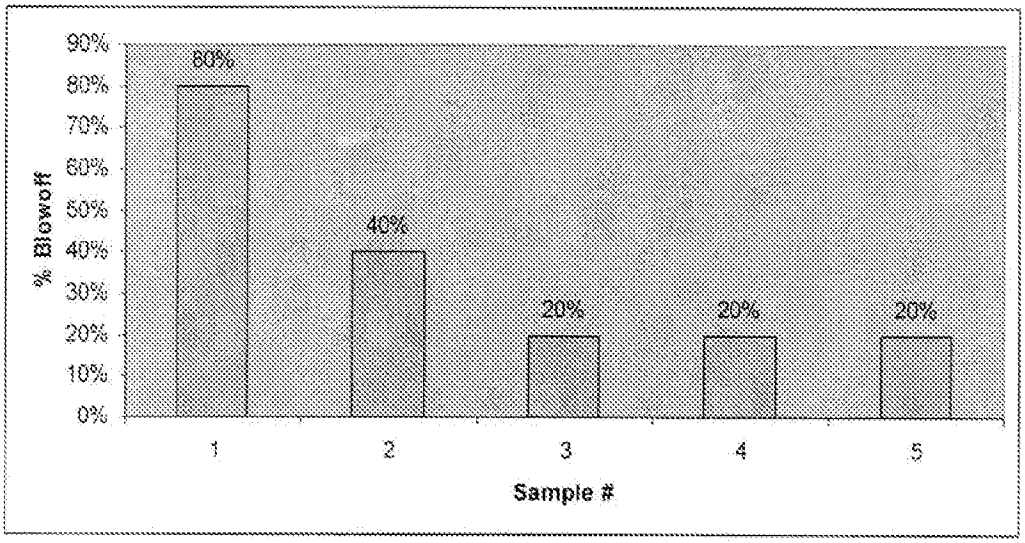
90%
80%
70%
60%
50%
40%
30%
20%
10%
0%
% Blowoff
80%
40%
20%
20%
20%
1
2
3
4
5
Sample #

FIG. 22

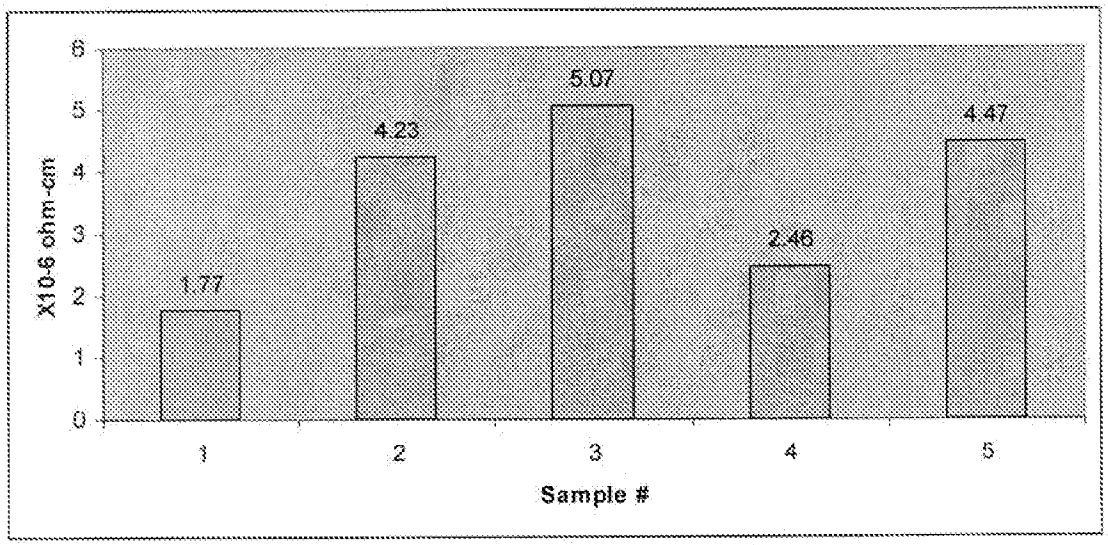

FIG 23

Sample #	Process
1	Standard
2	30 sec. microwave
3	1 min. microwave
4	2 min. microwave
5	3 min. microwave

FIG. 24

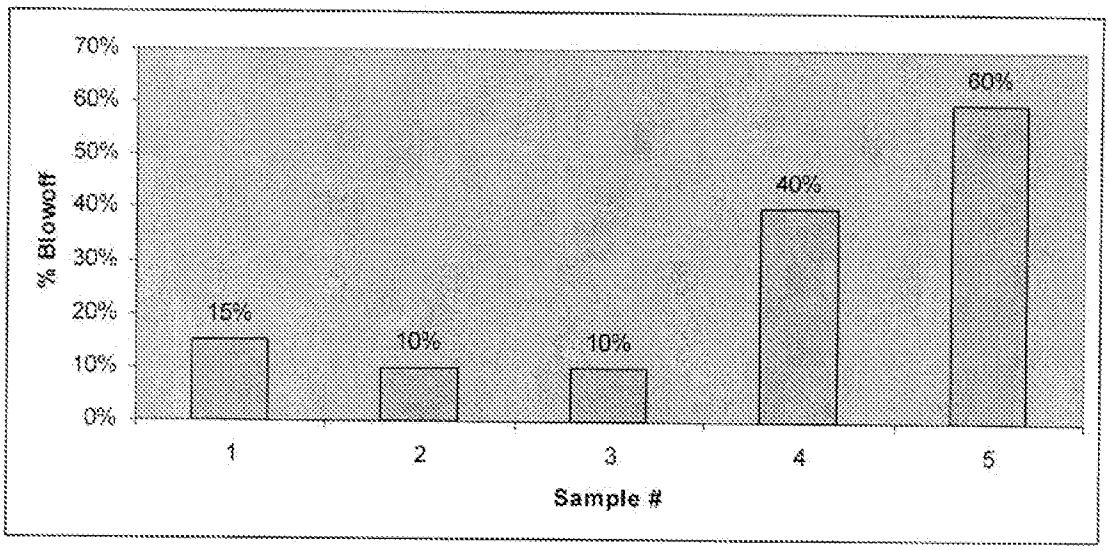

FIG. 25

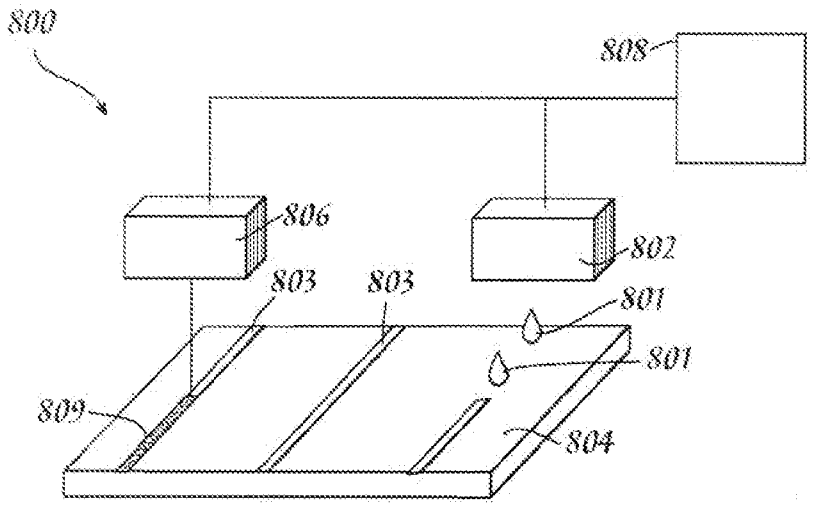

FIG. 26A

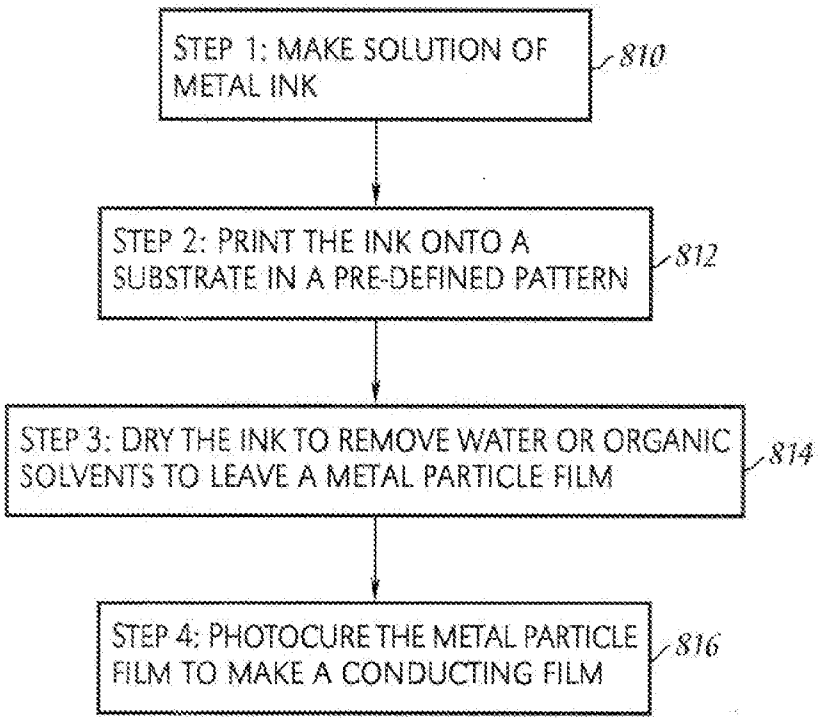

FIG. 26B

INTERNATIONAL SEARCH REPORT

International application No.
PCT/US 09/44195

A. CLASSIFICATION OF SUBJECT MATTER
IPC(8) - C09D 1/00 (2009.01)
USPC - 106/31.01
According to International Patent Classification (IPC) or to both national classification and IPC

B. FIELDS SEARCHED

Minimum documentation searched (classification system followed by classification symbols)
IPC(8) -- C09D 1/00 (2009.01) and USPC -- 106/31.01

Documentation searched other than minimum documentation to the extent that such documents are included in the fields searched
IPC(8) -- B22F3; B41M3/00 (2009.01) and USPC -- 106/31.01, 31.43; 252/500; 257/E23.074

Electronic data base consulted during the international search (name of data base and, where practicable, search terms used)
PubWest (PGPB,USPT,USOC,EPAB,JPAB); Espacenet; Google Patents; Google Scholar; Google -- please see extra sheet for Search Terms Used

C. DOCUMENTS CONSIDERED TO BE RELEVANT

Category*	Citation of document, with indication, where appropriate, of the relevant passages	Relevant to claim No.
Y	US 2003/0168639 A1 (Cheon et al.) 11 September 2003 (11.09.2003) para [0003]; [0006]; [0041]	1-5
Y	US 2007/0105395 A1 (Kinzel et al.) 10 May 2007 (10.05.2007) para [0014]; [0015]; [0016]; [0017]; [0028]	1-5
Y	US 2005/0148164 A1 (Casey et al.) 07 July 2005 (07.07.2005) [0017]; [0028]; [0029]	3
Y	US 6,010,771 A (Isen et al.) 04 January 2000 (04.01.2000) Fig 5; col 8, ln 1-20	5

☐ Further documents are listed in the continuation of Box C. ☐

* Special categories of cited documents:
"A" document defining the general state of the art which is not considered to be of particular relevance
"E" earlier application or patent but published on or after the international filing date
"L" document which may throw doubts on priority claim(s) or which is cited to establish the publication date of another citation or other special reason (as specified)
"O" document referring to an oral disclosure, use, exhibition or other means
"P" document published prior to the international filing date but later than the priority date claimed
"T" later document published after the international filing date or priority date and not in conflict with the application but cited to understand the principle or theory underlying the invention
"X" document of particular relevance; the claimed invention cannot be considered novel or cannot be considered to involve an inventive step when the document is taken alone
"Y" document of particular relevance; the claimed invention cannot be considered to involve an inventive step when the document is combined with one or more other such documents, such combination being obvious to a person skilled in the art
"&" document member of the same patent family

Date of the actual completion of the international search
18 June 2009 (18.06.2009)

Date of mailing of the international search report
25 JUN 2009

Name and mailing address of the ISA/US
Mail Stop PCT, Attn: ISA/US, Commissioner for Patents
P.O. Box 1450, Alexandria, Virginia 22313-1450
Facsimile No. 571-273-3201

Authorized officer:
Lee W. Young
PCT Helpdesk: 571-272-4300
PCT OSP: 571-272-7774

Form PCT/ISA/210 (second sheet) (April 2007)